ELSEVIER

Journal of Nuclear Materials 312 (2003) 134–140

journal of nuclear materials

www.elsevier.com/locate/jnucmat

Measurements of hydrogen permeation and absorption in zirconium oxide scales

Byung Hyuck Lim, Hyun Seon Hong *, Kyung Sub Lee

Division of Materials Science and Engineering, Hanyang University, 17 Huengdang-dong, Seongdong-ku, Seoul 133-791, South Korea

Received 24 July 2002; accepted 29 October 2002

Abstract

The hydrogen absorption and the permeation behavior through the oxide layer formed on modified Zircaloy-4 (Zry-4) alloys were investigated. The modified Zry-4 was prepared by altering the chemical composition of standard Zry-4. The tin content of Zry-4 (1.5 wt%) was reduced to 0.5 wt%, and alloying elements Si, O and Nb were added from 0.01 to 0.2 wt%. The oxide layers were grown in a static autoclave at 360 °C under 18.3 MPa for 150 days. Fick's law was used to calculate the diffusivity of hydrogen after the steady state of the permeation flux was reached. The diffusivity of hydrogen in the 0.5Sn–0.1Nb–0.1Fe–0.2Cr–0.2O–Zr specimen was lower than that in the 1.5Sn–0.2Fe–0.1Cr–0.1O–0.01Si–Zr and Zry-4 specimens. As the area fraction of precipitates increased, the hydrogen diffusivity increased whereas an inverse relationship between the diffusivity and the amount of the tetragonal phase was observed. In addition to the oxide structural study, the effects of the microstructure of the zirconium alloys such as precipitates and grain boundaries on the hydrogen absorption were studied.

1. Introduction

The recent trends of high fuel burn-up, extended recycle and high pH operation for increasing energy efficiency has led to the need to improve the corrosion resistance of Zircaloy-4 (Zry-4) cladding. Many efforts have been made to develop advanced cladding materials by altering the Zry-4 composition. The development of modified Zry-4 has been attempted by the authors through the addition of the alloying elements Si, O and Nb in Zry-4 [1–4]. The addition of small amounts of oxygen improved the mechanical properties of the cladding but degraded the oxidation resistance whereas the addition of silicon improved the oxidation resistance. However, the effect of these alloying elements on the hydrogen penetration behavior accompanied with the oxidation reaction has yet to be conducted.

The surface reaction of the fuel cladding with cooling water results in the oxidation of the cladding and the subsequent release of hydrogen. Some fraction of the released hydrogen is picked-up and diffuses into the Zircaloy matrix, causing the formation of hydrogen precipitates [5]. It is reported that the grain boundaries provide a transportation path for hydrogen diffusion while the microstructural defects such as precipitates and voids can affect the hydrogen pick-up rate [6,7]. It is also reported that oxide layers can hinder the hydrogen absorption in metals [8,9]. The electrochemical permeation is a reliable method used to investigate the hydrogen diffusion behavior through an oxide layer by applying a hydrogen concentration gradient. Many studies have been published using this method to study effects of microstructure, defect and surface condition on the permeation behavior in various metal-hydrogen systems [7,10]. However, the study on the hydrogen behavior in zirconium alloys using the electrochemical permeation method for cladding materials is scant.

In the present study, the hydrogen permeation behavior through oxidized Zry-4 and modified Zry-4 alloys

* Corresponding author. Tel.: +82-222 90 0382; fax: +82-222 82 4914/2281 4914.

E-mail address: hshong@ihanyang.ac.kr (H.S. Hong).

0022-3115/03/$ - see front matter
PII: S0022-3115(02)01556-8

after the oxidation at 360 °C under 18.3 MPa was investigated. The influences of grain size, precipitates and oxide layer on hydrogen permeation were evaluated. In addition, the hydrogen absorption characteristics of these alloys were studied.

2. Experimental procedures

2.1. Specimen preparation

Two types of modified Zry-4 alloys were prepared by altering the chemical composition of standard Zry-4. In the first type, the tin content of Zry-4 (1.5 wt%) was decreased to 0.5 wt%. The Fe/Cr ratio of Zry-4 reduced to 0.5. 0.1 wt% Nb and 0.2 wt% oxygen were added. In the second type, the tin content was maintained at 1.5 wt% and the Fe/Cr ratio was maintained at 2. 0.01 wt% Si was added. The chemical compositions of the specimens are listed in Table 1.

Sponge zirconium and the alloying elements were arc-melted into 200 g button-type ingots and remelted four times to achieve homogenization. After arc remelting, ingots were beta forged at 1100 °C and quenched in water. Forging was performed in the β temperature region to eliminate the casting structure. After β quenching, the specimens were hot-rolled at 700 °C followed by annealing at 650 °C under Ar atmosphere. The plates were then cold-rolled and annealed at 700 °C for 2 h for recrystallization.

2.2. Microstructural observation

The precipitates and grain size of the specimens were observed by optical microscopy and scanning electron microscopy (SEM). Specimens used in the experiments were pickled in a solution of 10 vol.% HF + 45 vol.% HNO_3 + 45 vol.% H_2O, prior to microstructure observations.

The specimens were oxidized for 150 days in static autoclaves filled with pure water at 360 °C under a pressure of 18.3 MPa. The oxidation behavior was evaluated by weight gain as a function of exposure time. XRD was used to observe the intensity of the tetragonal and monoclinic phases, and the thickness of the oxide layer was measured by SEM. Prior to XRD analysis, the specimens were ultrasonically cleaned in acetone and rinsed with distilled water. After mechanical polishing and pickling in a 10 vol.% HF + 45 vol.% HNO_3 + 45 vol.% H_2O solution, the Zr/ZrO_2 interface was observed by SEM.

2.3. Permeation test

The effective diffusivity of atomic hydrogen (D_{eff}) and the solubility (C_0) in oxidized Zry-4 alloys were measured by the electrochemical permeation test at room temperature. The permeability of each specimen was evaluated through the time lag (t_L) [11]. Hydrogen was introduced according to Devanathan and Statchurski's method [12,13]. The dimension of the specimen was 10 mm (W) × 20 mm (L) × 100 μm (T). The hydrogen entrance side of the specimen was polished to remove the oxide layer and then coated with Pd to reduce the dissolution of the Zircaloy matrix by reaction with the electrolyte.

For permeation tests, the cathode was filled with 5 M/ℓ KOH and hydrogen was charged at a galvanic current of 10 mA/cm^2. After hydrogen charging, a constant voltage of 1 V was applied to the anode and the change of the anodic current was monitored throughout the permeation test.

Fig. 1 shows the result of the Zry-4 specimen obtained from a permeation test. The steady state (t_S) was defined as the time corresponding to the intersection of the extrapolated initial and final linear portion of the permeation curve and t_L was defined as the time required for permeation to reach 63% of the current density at t_S (P_∞). The diffusion coefficient (D_{eff}) was calculated by the time-lag method [11],

$$D_{eff} = \frac{L^2}{6t_L}, \tag{1}$$

where D_{eff} (cm^2/s) is the effective diffusivity coefficient and L (cm) is the specimen thickness. The solubility (C_0) of hydrogen was obtained by the following equation,

Table 1
Chemical composition of the modified Zry-4 alloys and Zry-4 (in wt%)

Specimens	Alloy elements						
	Sn	Nb	Fe	Cr	O	Si	Zr
#1 (Zircaloy-4[a])	1.5	0.01	0.2	0.1	0.1	0	Bal
#2 (1.5Sn–0.2Fe–0.1Cr–0.1O–0.01Si–Zr[b])	1.5	0	0.2	0.1	0.1	0.01	Bal
#3 (0.5Sn–0.1Nb–0.1Fe–0.2Cr–0.2O–Zr[c])	0.5	0.1	0.1	0.2	0.2	0	Bal

[a] Denoted as Zry-4 in the text.
[b] Denoted as 0.01Si–Zr.
[c] Denoted as 0.5Sn–0.1Nb–0.2O–Zr.

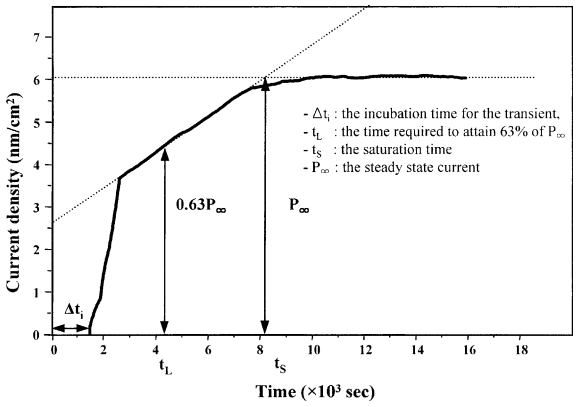

Fig. 1. The permeation curve of Zry-4 obtained from permeation test.

$$C_0 = \frac{J_\infty L}{D_{\text{eff}} F}, \tag{2}$$

where C_0 (mol/cm^3) is the hydrogen solubility in the specimens, J_∞ (μA/cm^2) is the current density at the steady-state, and F is the Faraday's constant.

3. Results and discussion

3.1. Oxidation behavior

Fig. 2 shows the weight gain and oxide thickness changes of Zry-4 and the modified Zry-4 as a function of exposure time. It can be seen that the Zry-4, 1.5Sn–0.2Fe–0.1Cr–0.1O–0.01Si–Zr (0.01Si–Zr) and 0.5Sn–0.1Nb–0.1Fe–0.2Cr–0.2O–Zr (0.5Sn–0.1Nb–0.2O–Zr) specimens had similar weight gains over the 150 days of oxidation. Subsequently, the oxide thickness of the specimens were similar (3.8 ± 0.1) μm. The thickness was measured at three random points along the specimens by SEM. From the surface observation, it was found that the oxides were uniformly black and compact. It was reported in previous studies [1–4] that the addition of small amounts of oxygen degraded the oxidation resistance while additions of Nb and Si improved the oxidation resistance. Due to the compositions of the three specimens, it was expected that they would experience different weight gains. However, it was possible that the specimens in the current study had similar weight gains due to the overall influence of each alloying element.

In terms of alloying effects on oxidation, it should be noted that in the present study the weight gains resulted from short-term exposure. Long-term effects could be different from short-term oxidation, that is, it is possible that the oxidation characteristics of Zyr-4 and the modified Zry-4 alloys are changed during the longer exposure. In this study, long-term experiments over 150 days have not been performed because the formation of 3–4 μm thick oxides was enough for the present propose of permeation tests.

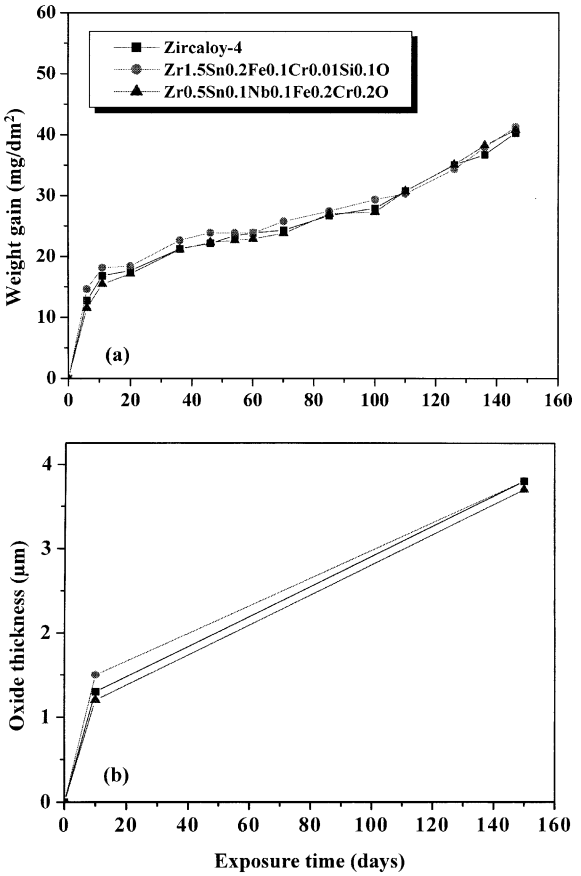

Fig. 2. Weight gain and oxide thickness of the alloys as a function of exposure time.

3.2. Hydrogen permeation behavior

The hydrogen diffusivity and solubility of each specimen were measured by electrochemical permeation. The hydrogen diffusivity in the specimens was calculated by Eq. (1). The diffusivity in the 0.5Sn–0.1Nb–0.2O–Zr specimen was found to be 1.26×10^{-8} cm^2/s which was smaller than those in Zry-4 (1.51×10^{-8} cm^2/s) and the 0.01Si–Zr specimen (1.49×10^{-8} cm^2/s). In this study, the effects of the precipitates and grain boundaries on the diffusivity were investigated by microstructure observations. The matrix grain of the specimens, the distribution of precipitates in matrix and the oxide grain morphology are shown in Fig. 3. The values of the average grain size and the area fraction of precipitates are summarized in Table 2. Mainly columnar oxide grains

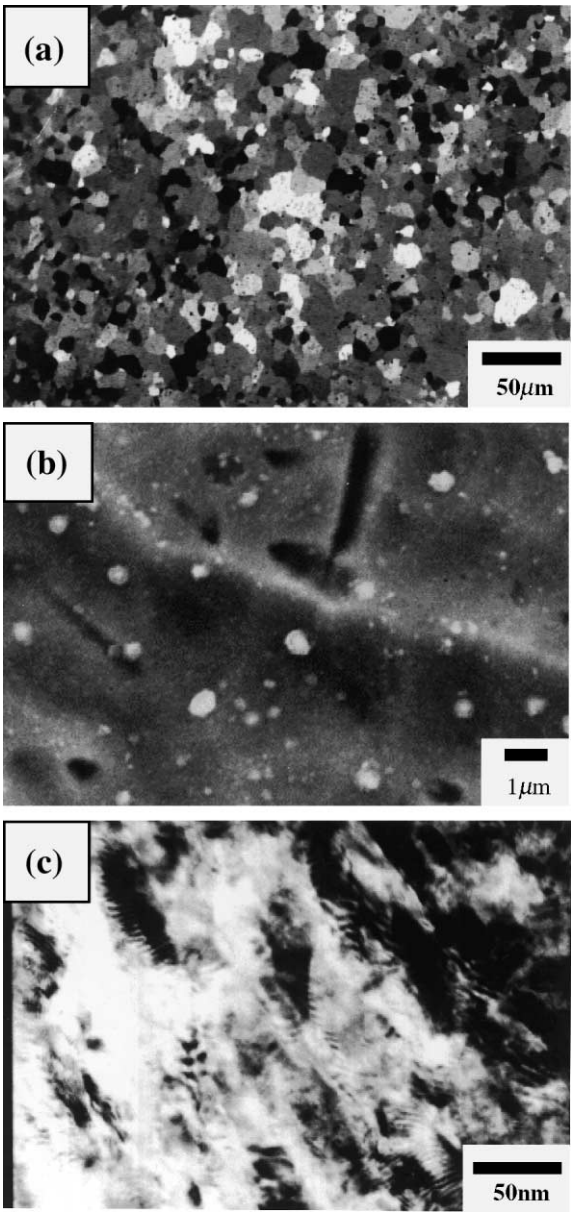

Fig. 3. The microstructure of (a) the equiaxed grain of the 0.01Si–Zr specimen, (b) the precipitates in the 0.01Si–Zr specimen and (c) the columnar grains of the oxide in the 0.01Si–Zr specimen.

were found from the oxide observation and the size of the columnar grains ranged from 50 to 200 nm as shown in Fig. 3(c). Equiaxed grains were also observed near the oxide surface. However, these grains showed the irregular distribution and the amount was small. The diffusivity changes with the grain size, the area fraction of precipitates and the relative fraction of tetragonal ZrO_2 are listed in Table 3. It is considered from the table that the influence of grain size on the diffusivity change is unclear, however, the area fraction did affect the diffusivity. The higher area fraction resulted in a lower diffusivity.

It is well known that the intermetallic precipitates are more noble than the zirconium matrix [14–18]. Thus, the precipitates in a metallic state are accommodated in the oxide and then gradually oxidized. It is also known that electrons, produced by the oxidation reaction at the metal/oxide interface, move toward the oxide surface through the intermetallic precipitates in the oxide [19–21]. The precipitates in direct contact with the matrix or by forming a network tend to be negatively charged. A chain-like distribution of precipitates may be seen in Fig. 3(b). These charged precipitates are thought to interact with hydrogen ions acting as trapping sites. Consequently, it is suggested that the precipitates in a metallic state have the large electrical affinity to hydrogen, and hence absorbed hydrogen in the oxide was trapped at the precipitates, rendering that the specimens with higher precipitate fractions had lower diffusion coefficients such as in the present study.

In order to study the effect of the ZrO_2 microstructure on hydrogen diffusion, the structural analysis of the oxides was carried out by SEM and XRD. The semi-analytic method by Gravie and Nicholson [22] was used to calculate the fraction of tetragonal ZrO_2:

$$\text{Relative fraction of tetragonal-}ZrO_2 = \frac{I(1\,1\,1)_t}{I(-1\,1\,1)_m + I(1\,1\,1)_m + I(1\,1\,1)_t}. \quad (3)$$

It was found that the oxides of Zry-4 and modified Zry-4 were composed of the tetragonal and monoclinic phases in the pre-transition region. The relative fraction of tetragonal-ZrO_2 was less after 150 days exposure than it was at 10 days exposure. According to Godlewski

Table 2
Average grain size of zirconium matrix and area fraction of precipitates in Zr-based alloys

Specimens	Average size of matrix grains (μm)	Average size of precipitates (μm)	Area fraction of precipitates (%)
#1 (Zry-4)	17.6	1.2	2.0
#2 (1.5Sn–0.2Fe–0.1Cr–0.1O–0.01Si–Zr)	14.8	1.2	2.2
#3 (0.5Sn–0.1Nb–0.1Fe–0.2Cr–0.2O–Zr)	20.3	1.4	2.7

Table 3
Comparisons of diffusion coefficients with average grain size, area fraction of precipitates and the relative tetragonal phase fraction in Zr alloys at 298 K

Specimens	Diffusivity (cm^2/s)	Average size of matrix grains (μm)	Area fraction of precipitates (%)	Relative tetragonal phase fraction (%)
#1 (Zry-4)	1.51×10^{-8}	17.6	2.0	10.9
#2 (1.5Sn–0.2Fe–0.1Cr–0.1O–0.01Si–Zr)	1.49×10^{-8}	14.8	2.2	12.0
#3 (0.5Sn–0.1Nb–0.1Fe–0.2Cr–0.2O–Zr)	1.26×10^{-8}	20.3	2.7	15.3

[23,24], the tetragonal phase is stabilized by the compressive stress in the oxide. As the compressive stress is relaxed during outward growth of the oxide, the tetragonal phase becomes destabilized and transforms to the monoclinic phase.

The structure of ZrO_2, evaluated by XRD on the specimens exposed for 150 days, showed that the amount of the tetragonal phase was in the range 10.8–15.3% in Zry-4 and modified Zry-4; the fraction of tetragonal ZrO_2 of the 0.5Sn–0.1Nb–0.2O–Zr specimen (15.3%) was higher than that of Zry-4 (10.8%) and the 0.01Si–Zr (11.5%) specimen.

The inverse relationship was observed between the relative fraction of tetragonal ZrO_2 and hydrogen diffusivity as can be seen in Table 3; the diffusivity decreased as the fraction increased. This inverse relationship can be explained as follows. During the oxide growth, tetragonal ZrO_2 became destabilized and changed to monoclinic ZrO_2. This tetragonal-to-monoclinic transition was governed by a martensitic transformation, resulting in microcracks around twin boundaries [25]. It is considered that interconnected microcracks could provide fast transport routes of hydrogen through the oxide layer. Accordingly, the low fraction of tetragonal ZrO_2 exhibited the high diffusivity in the present study. The role of intermetallic precipitates and microcracks in hydrogen transport mechanism is schematically presented in Fig. 4. The average precipitate size in the present specimens was around 120 nm (see Table 2). The oxide grains in the present specimen were found to have mainly columnar structure ranging from 50 to 200 nm (see Fig. 3). Equiaxed grains were also observed near the oxide surface, however, the fraction of the equiaxed grains to the columnar grains was low and the distribution was irregular. Similarly, Oskarsson et al. [26] reported that columnar grains of the oxide were observed for the oxidation of Zry-2 at 360 °C in water. The average size of the columnar grains was around 150 nm. The columnar grains with 200 nm length were also reported in Zr–2.5Nb alloys after the steam oxidation at 400 °C [27]. These values of the grain sizes and precipitates were referred in Fig. 4. It is to be noted that hydrogen ions could diffuse via the pore network of up to 10 nm wide following the grain boundaries of the oxide [27] as well as the microcrack network around twin boundaries. The average grain size of the oxides is smaller than that of the matrix by a factor of 10 as shown in Fig. 4 so the pore networking around the grain boundaries in the oxide seems to provide fast routes for diffusion as well as the microcracks. Large cracks with the length of around 100 nm lying parallel to the oxide surface were occasionally observed in the bulk oxide but this feature is not illustrated in Fig. 4.

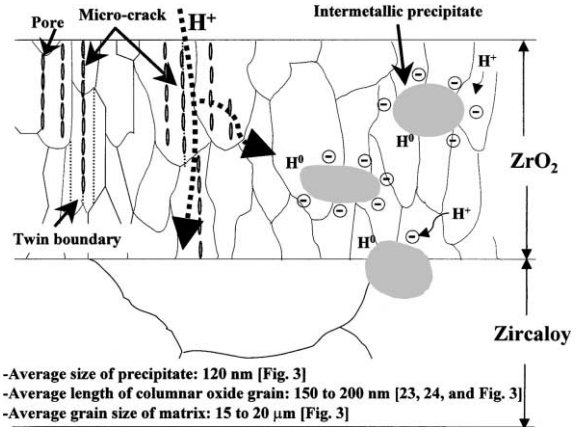

Fig. 4. Schematic diagram of the roles of precipitates and interconnected microcracks in the hydrogen transport process.

It is probable that the oxygen diffusion was also affected by the fraction of tetragonal ZrO_2 during the oxidation. The relationship was not delineated between the oxygen diffusion and the fraction of tetragonal ZrO_2 in this study. However, it is likely that the hydrogen ion is more sensitive to the oxide structure than the oxygen ion when they diffuse through the oxide layer because the diffusivity of hydrogen was fairly dependent on the fraction of the tetragonal phase as seen in the present results whereas the oxygen diffusion was not affected so much as hydrogen.

3.3. Hydrogen absorption characteristics

The hydrogen solubility in Zry-4, determined by Eq. (2), showed the highest value of 4.8×10^{-5} mol/cm^3

Table 4
Diffusivity and solubility of hydrogen in Zr-based alloys after 150 days exposure at 298 K

Specimens	Diffusivity (cm^2/s)	Solubility (mol/cm^3)
#1 (Zry-4)	1.51×10^{-8}	4.76×10^{-5}
#2 (1.5Sn–0.2Fe–0.1Cr–0.1O–0.01Si–Zr)	1.49×10^{-8}	3.20×10^{-5}
#3 (0.5Sn–0.1Nb–0.1Fe–0.2Cr–0.2O–Zr)	1.26×10^{-8}	3.48×10^{-5}

Table 5
Hydrogen uptake, pickup fraction and solubility in Zr alloys after permeation test at 298 K

Specimens	Hydrogen uptake (ppm)	Hydrogen pickup fraction (%)	Solubility (mol/cm^3)
#1 (Zry-4)	170	8.0	4.76×10^{-5}
#2 (1.5Sn–0.2Fe–0.1Cr–0.1O–0.01Si–Zr)	102	4.8	3.20×10^{-5}
#3 (0.5Sn–0.1Nb–0.1Fe–0.2Cr–0.2O–Zr)	114	5.1	3.48×10^{-5}

among the present specimens. The solubilities in the 0.01Si–Zr specimen and the 0.5Sn–0.1Nb–0.2O–Zr specimen were 3.2×10^{-5} mol/cm^3 and 3.5×10^{-5} mol/cm^3, respectively. The values of diffusivity and solubility after permeation are listed in Table 4. It is known that the hydrogen absorption characteristics are sensitive to the alloying elements in Zry [28,29]. For example, Ni contents in Zry-2 used in BWR increase the hydrogen absorption rate. In this study, it was proposed that the alloying elements such as Nb, O and Si in the specimens affected the absorption of hydrogen. Therefore, the hydrogen uptake and pick-up fraction in the specimens were analyzed. The hydrogen uptake was defined as the amount of hydrogen accumulated in the specimens due to the oxidation. In this study, the hydrogen uptake was experimentally obtained by the extraction method. On the other hand, the hydrogen pick-up fraction was defined as the ratio of the measured hydrogen concentration in the specimen to the hydrogen theoretically generated by the oxidation reaction. The value of hydrogen uptake was used for the measured hydrogen concentration while the theoretical amount of hydrogen was obtained by calculating the hydrogen amount from the weight gains in the present specimens.

Table 5 shows a comparison of the hydrogen uptake with the hydrogen pick-up fraction and solubility. The hydrogen pick-up fraction was in proportion to the hydrogen uptake because the present specimens had similar weight gains during the 150 days of oxidation. However, the hydrogen uptake in Zry-4 was higher than those in 0.01Si–Zr and 0.5Sn–0.1Nb–0.2O–Zr. The solubility calculated from permeation tests showed a similar distribution to the hydrogen uptake obtained from the extraction methods. Consequently, it is considered that the addition of Si, Nb and oxygen in the modified Zry-4 enhanced the hydrogen absorption resistance compared to Zry-4.

4. Conclusion

1. Three to four micrometer thick oxides for permeation experiments were grown on Zry-4, 0.01Si–Zr and 0.5Sn–0.1Nb–0.2O–Zr specimens by oxidation in pure water in a static autoclave at 360 °C for 150 days. The oxides were apparently uniformly black and compact. It was found from the microstructural study that the oxides were composed of tetragonal and monoclinic ZrO_2. The amount of the tetragonal phase was largest in the 0.5Sn–0.1Nb–0.2O–Zr specimen.
2. The diffusivity of hydrogen in the oxidized zirconium alloys measured by permeation tests showed that the diffusivity in the 0.5Sn–0.1Nb–0.2O–Zr specimen was smaller than that in Zry-4 and the 0.01Si–Zr specimens. The diffusivity appeared to depend on the area fraction of precipitates and the amount of tetragonal ZrO_2. These results were explained by modeling that the precipitates in a metallic state acted as trapping sites while the tetragonal-to-monoclinic transition provided the fast transport route of hydrogen.
3. The solubility of hydrogen in Zry-4 was higher than that in the 0.5Sn–0.1Nb–0.2O–Zr and 0.01Si–Zr specimens. This hydrogen absorption behavior was confirmed by the hydrogen pick-up fraction and hydrogen up-take obtained from the hydrogen extraction analysis. Thus, it is considered that alloying elements such as Si, Nb and oxygen in the modified Zry-4 alloys affected the hydrogen absorption behavior.

Acknowledgements

This study was supported by Korea Institute S&T Evaluation and Planning (KISTEP) and Brain Korea 21 (BK21) Foundation.

References

[1] H.S. Hong, S.J. Kim, K.S. Lee, J. Nucl. Mater. 236 (1996) 211.
[2] H.S. Hong, S.J. Kim, K.S. Lee, J. Nucl. Mater. 280 (2001) 230.
[3] H.S. Hong, S.J. Kim, K.S. Lee, J. Nucl. Mater. 297 (2001) 113.
[4] H.S. Hong, S.J. Kim, K.S. Lee, J. Nucl. Mater. 304 (2002) 8.
[5] Y.S. Kim, D.R. Olander, J. Kor. Nucl. Mater. 25 (1993) 570.
[6] X.Y. Chang, X.J. Wan, Scripta Mater. 38 (1998) 1505.
[7] A.M. Bress, A. Chanfreau, Acta Mater. 44 (1996) 3823.
[8] R.H. Song, S.I. Pyun, R.A. Oriani, J. Electrochem. Soc. 137 (1990) 1703.
[9] M.J. Danielson, Corros. Sci. 44 (2002) 829.
[10] P. Manolatos, M. Jerome, C. Duret-thual, J. Le Coze, Corros. Sci. 37 (1995) 173.
[11] J. McBreen, L. Nanis, W. Beck, J. Electrochem. Soc. 113 (1966) 1218.
[12] M.A.V. Devanathan, Z. Stachurski, Proc. Roy. Soc. London, Ser. A 270 (1962) 90.
[13] M.A.V. Devanathan, Z. Stachurski, J. Electrochem. Soc. 111 (1964) 619.
[14] Y. Hatano, K. Isobe, R. Hitaka, M. Sugisaki, J. Nucl. Sci. Technol. 33 (1996) 944.
[15] Y. Hatano, R. Hitaka, M. Sugisaki, M. Hayashi, J. Nucl. Mater. 248 (1997) 311.
[16] D. Khatamian, J. Alloys Comp. 231 (1995) 722.
[17] B. Cox, J. Alloys Comp. 256 (1997) L4.
[18] N. Ramasubramanian, in: Proceedings of IAEA Technical Committee Meeting on Fundamental Aspects of Corrosion of Zirconium-Based Alloys in Water Reactor Environments, IWGFPT/34, IAEA, Vienna, 1990, p. 36.
[19] T. Kubo, M. Uno, 9th International Symposium on Zirconium in the Nuclear Industry, vol. 1132, ASTM STP, 1991, p. 476.
[20] D. Shaltiel, I. Jacob, D. Davodov, J. Less-Common Met. 53 (1977) 117.
[21] D.F. Taylor, B. Cheng, R.B. Adamson, in: Proceedings of IAEA Technical Committee Meeting on Fundamental Aspects of Corrosion of Zirconium-Based Alloys in Water Reactor Environments, IWGFPT/34, IAEA, Vienna, 1990, p. 27.
[22] R.C. Garvie, P.S. Nicholson, J. Am. Ceram. Soc. 55 (1972) 303.
[23] J. Godlewski, J.P. Gros, M. Lambertin, J.F. Wadier, H. Weidinger, in: 9th International Symposium on Zirconium in the Nuclear Industry, vol. 1132, ASTM STP, 1991, p. 416.
[24] J. Godlewski, in: 10th International Symposium on Zirconium in the Nuclear Industry, vol. 1245, ASTM STP, 1994, p. 663.
[25] B. Cox, Atomic Energy of Canada Ltd., Report AECL-9382, 1987.
[26] M. Oskarsson, E. Aflberg, U. Andersson, K. Pettersson, J. Nucl. Mater. 297 (2001) 77.
[27] B.D. Warr, M.B. Elmoselhi, S.B. Newcomb, N.S. McIntyre, A.M. Brennenstuhl, P.C. Lichtenberger, in: 9th International Symposium on Zirconium in the Nuclear Industry, vol. 1132, ASTM STP, 1991, p. 740.
[28] V.K. Sinha, J. Nucl. Mater. 59 (1976) 201.
[29] Y.S. Kim, S.K. Kim, J.G. Bang, Y.H. Jung, J. Nucl. Mater. 279 (2000) 335.